

Logistic-Gated Operators Enable Auditable Unit-Aware Thresholds in Symbolic Regression

Ou Deng^{1*}, Ruichen Cong², Jianting Xu¹, Shoji Nishimura², Atsushi Ogihara², and Qun Jin²

¹Graduate School of Human Sciences, Waseda University. Tokorozawa, Saitama 359-1192, Japan

²Faculty of Human Sciences, Waseda University. Tokorozawa, Saitama 359-1192, Japan

*Correspondence: dengou@toki.waseda.jp

Bigger Picture

AI for health will only scale when outputs are readable, auditable, and governable. Many clinical and biological decisions hinge on thresholds — cut-points that trigger action — yet most models bury them behind opaque scores. We introduce logistic-gated operators (LGO) for symbolic regression, which treat thresholds as first-class, unit-aware parameters inside equations and map them back to physical units for direct comparison with guidelines. This reframes interpretability from a post-hoc narrative into a modeling constraint, yielding compact formulas that clinicians can inspect, audit, and deploy. LGO’s gates are selective and parsimonious — used when regime switching matters and pruned when relations are smooth — offering a practical path to governance-ready AI. As standalone primitives or a safety overlay on black-box systems, LGO helps translate data into auditable, unit-aware rules for medicine and beyond.

Highlights

- **Unit-aware auditability:** thresholds are explicit inside symbolic equations and inverted to physical units for guideline comparison and governance.
- **Parsimony by design:** hard/soft gates favor sparse, compact formulas and automatically prune when thresholds are not warranted.
- **Typed, stable pipeline:** standardized-space training with train-only inversion and strong typing supports reliable search and threshold recovery.
- **Flexible deployment:** usable as a standalone primitive or an auditable safety overlay on black-box models in health and other domains.

Summary

Symbolic regression promises readable equations but struggles to encode unit-aware thresholds and conditional logic. We propose logistic-gated operators (LGO) — differentiable gates with learnable location and steepness — embedded as typed primitives and mapped back to physical units for audit. Across two primary health datasets (ICU, NHANES), the hard-gate variant recovers clinically plausible cut-points: ~71% (5/7) of assessed thresholds fall within 10% of guideline anchors and 100% within 20%, while using far fewer gates than the soft variant (ICU median 4.0 vs 10.0; NHANES 5.0 vs 12.5), and remaining within the competitive accuracy envelope of

strong SR baselines. On predominantly smooth tasks, gates are pruned, preserving parsimony. The result is compact symbolic equations with explicit, unit-aware thresholds that can be audited against clinical anchors — turning interpretability from a post-hoc explanation into a modeling constraint and equipping symbolic regression with a practical calculus for regime switching and governance-ready deployment.

Keywords

Symbolic Regression, Genetic Programming, Logistic-Gated Operators, Unit-Aware Thresholds, Model Auditability, Interpretable Machine Learning, Regime Switching, Clinical Decision Support, Critical Care (ICU), Cardiometabolic Risk

Introduction

Motivation and background.

Symbolic regression (SR) searches for analytic expressions that explain data-generating mechanisms and, crucially for high-stakes settings, expose testable assumptions^{1,2}. In contrast to black-box predictors, SR can return compact formulas whose parameters admit scientific interpretation and regulatory traceability^{3,4}. In medicine and public health, this need goes beyond “readability”: clinicians and regulators routinely ask where the decision boundary lies, in what physical units, and how it compares to domain anchors or guidelines^{5,6}. Examples include mean arterial pressure (MAP) targets in sepsis care^{7,8}, blood-pressure tiers for cardiovascular risk management⁹, lipid and metabolic cut-points^{10,11}, and glucose thresholds used for screening/diagnosis¹². Governance documents likewise emphasize auditable, well-calibrated models with transparent update pathways¹³.

Two data ecosystems make these requirements concrete. First, critical-care EHR cohorts (e.g., MIMIC-IV) enable outcome modeling from routinely measured physiologic signals^{14–16}. Many of these variables — MAP, lactate, respiratory rate — have operational or guideline thresholds, so recovered turning points must be auditable in natural units. Second, population surveys such as NHANES provide nationally representative measurements of cardiometabolic risk factors where anchors (e.g., systolic BP tiers, HDL minima, waist-circumference bands, fasting-glucose ranges) are embedded in screening programs^{17,18}. In both settings, beyond accuracy, stakeholders value models that use as few switches as necessary and that make those switches explicit for clinical review¹⁹.

Classical SR approximates thresholded behavior indirectly by composing arithmetic and smooth primitives. This can fit data but often produces long expressions with implicit cut-points that are hard to audit. Motivated by this gap, we propose a family of Logistic-Gated Operators (LGOs): symbolic primitives that encode gating with learnable location and steepness in standardized space and map back to physical units for audit. Our empirical focus is deliberately health-centric (ICU and NHANES), and our goal is not to chase single-number SOTA; rather, we target executable interpretability: unit-aware thresholds and sparse switching structure that clinicians and engineers can verify against guidance^{3,4}.

Related work and limitations.

Symbolic regression families and search heuristics. SR originated in genetic programming (GP), which evolves expression trees over primitive sets^{1,20,21}. Discoveries of compact laws and invariants demonstrated SR’s scientific promise². Subsequent work broadened search and selection, from strong typing and semantic constraints to selection schemes tailored for regression^{22,23}. Contemporary surveys benchmark diverse engines and highlight the trade-off space between fit and parsimony²⁴. Production-grade toolchains increasingly standardize operators and fitness reporting (e.g., Operon, PSTree, PySR, RILS–ROLS)^{25–28}.

Hybrid, differentiable, and neuro-symbolic approaches. Beyond evolutionary search, hybrid SR injects gradients, priors, or neural scaffolds to improve data efficiency and extrapolation. Physics-inspired pipelines and differentiable surrogates exemplify this direction^{29,30}. Deep symbolic regression and neural–symbolic integrations further leverage policy gradients and representation learning^{31,32}. Program-structure priors and grammar models guide the hypothesis space^{33,34}, while differentiable architecture search influences operator choice³⁵. These systems typically optimize expressions but do not return unit-aware thresholds as first-class parameters within the final symbolic model.

Gating and piecewise mechanisms. Decades of neural modeling underscore the value of gates for regime switching (e.g., LSTM/GRU) and specialization (mixture-of-experts)^{36–38}. Theoretical analyses of partitioning capacity (e.g., linear-region counts) clarify how gated compositions encode piecewise structure³⁹. LGO draws on this heritage but relocates gates into symbolic expressions whose parameters are trained in z-score space and then inverted to natural units, enabling direct audit against anchors.

Interpretable learners and post-hoc explanations. Rule lists, soft decision trees, and inherently interpretable models offer explicit conditional or additive structure^{40–42}. Model-agnostic toolkits provide local/global attributions and partial effects. However, these approaches either do not produce free-form analytic formulas interleaving gates with algebra, or they treat thresholds as implicit artifacts of the explainer. LGO instead makes thresholds part of the expression tree—with audited parameters—so they can be compared numerically to clinical or engineering anchors.

Scientific ML and operator learning. Symbolic discovery connects naturally to physics-informed and operator-learning frameworks that encode structure and units^{43,44}. Neural operator families and universal-approximation results underscore the value of parameterized kernels with semantic meaning (e.g., periods, diffusion scales)^{45–47}. Domain-equivariant architectures further illustrate how inductive bias can be aligned with scientific symmetries⁴⁸. LGO follows the same philosophy, but for thresholds: the parameters (a, b) are given explicit roles (steepness and location) and are audited back to physical units.

Health data, anchors, and governance. We evaluate on public cohorts with documented variable definitions (MIMIC-IV, NHANES)^{14–17} and anchor sets reflecting guideline practice: sepsis hemodynamic targets^{7,8}, blood pressure and lipid management^{9,10}, metabolic syndrome criteria¹¹,

and glucose classification standards¹². Such alignment facilitates clinical review and regulatory dialogue^{6,13}. For non-clinical benchmarks (CTG, Cleveland, Hydraulic), we reference UCI repositories for precise feature definitions^{49–51}.

Evaluation practice and sensitivity. Our protocol reports $\text{mean} \pm \text{std}$ across seeds and audits thresholds via natural-unit inversion, accompanied by sanity checks ($\text{RMSE} \geq \text{MAE}$; internal–external metric consistency). We use variance-based sensitivity tools when appropriate to probe stability^{52,53}. For causal interpretability and data issues (e.g., confounding, missingness), we draw on established literatures to inform audit and robustness practices^{54–56}.

Where LGO fits – and its limits. Compared with arithmetic-only SR^{1,24} and neuro-symbolic pipelines^{29,30}, LGO contributes unit-aware, auditable gates as primitives. The hard-gate variant typically yields sparser switching than a soft multiplicative gate, aligning with our target use-cases in ICU and NHANES. Limitations persist: on globally smooth relations (e.g., Hydraulic), gates may over-parametrize; anchors must be curated carefully (counts/categorical codes or age-dependent “normals” can mislead); and budgets for learning (a, b) matter. These boundaries argue for a mechanism-aware choice of primitives and for reporting both accuracy and parsimony³. Emerging SR directions — concept libraries, interactive co-design, and robustness studies — are complementary and can further benefit from making thresholds first-class, auditable objects^{57–61}.

Our proposal: Logistic-Gated Operator (LGO) family.

To close the expressivity–auditability gap, we enrich the SR primitive set with logistic-gated operator (LGO) that bring smooth gates and explicit thresholds into the symbolic search itself. We refer to the primitive as a LGO. Throughout, “unit-aware” denotes physical measurement units (mmHg, mmol/L, mg/dL), not the notion of “unit” as in “operator”. We adopt two canonical forms:

$$\text{LGO}_{\text{soft}}(x; a, b) = x \sigma(a(x - b)), \quad \sigma(z) = \frac{1}{1 + e^{-z}}, \quad (\text{Equation 1})$$

$$\text{LGO}_{\text{hard}}(x; a, b) = \sigma(a(x - b)). \quad (\text{Equation 2})$$

Here $b \in \mathbb{R}$ encodes a threshold and $a > 0$ controls transition steepness. Equation 1 preserves magnitude while gating (soft gate); Equation 2 isolates a probabilistic gate (hard tendency). LGOs are closed under composition: replacing x with a subexpression $f(x)$ yields expression-level gating $f(x) \sigma(a(f(x) - b))$; multi-input gates arise via products/sums of sigmoids, e.g., $\text{AND}_2(x, y) = \sigma(a(x - b)) \sigma(a(y - b))$ and $\text{OR}_2(x, y) = 1 - (1 - \sigma(a(x - b))) (1 - \sigma(a(y - b)))$.

We integrate LGOs into a strongly typed SR search to separate feature inputs (Feat), positive steepness (Pos) and thresholds (Thr), thereby constraining the hypothesis space and enabling targeted mutations on (a, b) ^{1,21,22}.

Theoretical properties and inductive bias.

Heaviside limit and calibration. For fixed b , $\sigma(a(x - b)) \rightarrow \mathbf{1}_{\{x > b\}}$ pointwise as $a \rightarrow \infty$; on any compact set avoiding $x = b$, the convergence is uniform. Hence LGO_{hard} approaches a step and LGO_{soft} approaches $x \mathbf{1}_{\{x > b\}}$. The parameter a therefore calibrates gate sharpness from graded modulation to near-discrete switching.

Smoothness, gradients, and regularization. Both gates are differentiable for finite a ; for Equation 1,

$$\frac{\partial}{\partial b} \text{LGO}_{\text{soft}}(x; a, b) = -a x \sigma(a\Delta)(1 - \sigma(a\Delta)), \quad \frac{\partial}{\partial a} \text{LGO}_{\text{soft}}(x; a, b) = x \Delta \sigma(a\Delta)(1 - \sigma(a\Delta)),$$

where $\Delta = x - b$. The gating factor has global Lipschitz constant $\leq a/4$ in x , which spreads transitions unless the data support sharp changes. This yields an implicit regularization bias toward smooth regime boundaries, tightened as a grows. The full operator list and properties are described in Section S2 of Supplemental Information.

Approximation of piecewise structure. Sigmoids approximate indicators and thus arbitrary continuous functions via superpositions^{62,63}. Combining this with multiplicative masking implies a constructive approximation for piecewise- C^1 maps: given k distinct thresholds on one dimension, there exists an LGO expression with $O(k)$ sigmoid factors whose uniform error on compact subsets (excluding the discontinuity loci) can be made arbitrarily small. In multiple dimensions, products of sigmoids approximate indicators of axis-aligned polytopes, enabling smooth partitioning of the domain into regimes subsequently modeled by simple algebraic subexpressions. Thus, LGOs endow SR with a direct “threshold calculus” instead of relying on lengthy arithmetic surrogates^{2,29}.

Typed semantics and search economy. Typing (Feat, Pos, Thr) restricts where each symbol may appear and confines (a, b) to their appropriate domains. This prunes invalid trees, improves search efficiency, and supports micro-mutations focused on (a, b) while preserving global structure^{22,23}. In turn, the hard gate induces a bias toward parsimonious switching (fewer active gates), while the soft gate favors graded modulation — an inductive bias we verify empirically on ICU and NHANES.

Unit-aware threshold recovery.

Expressions are evolved in standardized (z -score) space for numerical stability and comparability across features. For a feature x with training statistics (μ_x, σ_x) , a learned threshold \hat{b}_z maps back to natural units via

$$\hat{b}_{\text{raw}} = \mu_x + \sigma_x \hat{b}_z.$$

This unit-aware inversion is performed with train-only statistics to avoid leakage and enables direct audit against domain anchors (e.g., MAP 65 mmHg, lactate 2 mmol/L, SBP tiers, HDL minima, fasting-glucose ranges)^{8–12}. For expression-level gates $f(x) \sigma(a(f(x) - b))$, we estimate the z -standardization of $f(x)$ on the training fold and apply the same inversion principle.

Contributions.

We introduce LGOs as unit-aware, auditable gating primitives for SR and analyze their limiting, smoothness, and approximation properties. We design a typed, hybrid search with explicit (a, b) optimization and train-only inversion to natural units. On ICU and NHANES, LGO_{hard} yields sparser switching with thresholds that align with clinical anchors, while remaining competitively accurate within the SR landscape.

Paper organization.

Methods detail the LGO family, typing, and training/inversion pipeline; Experiments cover datasets, protocols, and SOTA baselines; Results report overall accuracy, threshold audits, parsimony and ablations; Discussion reflects on governance, deployment, and limitations.

Results

Overall predictive performance across datasets

We first summarize predictive accuracy across methods and datasets to situate LGO within the current symbolic-regression landscape. Figure 1 visualizes the distribution of performance over up to ten random seeds per method and dataset (Hydraulic excludes two anomalous seeds (R^2 for regression, AUROC for CTG); see SI Table S10). Each violin encodes the full seed distribution, black dots mark individual runs, and the numbers beneath each violin report the mean \pm standard deviation across seeds.

Across datasets, RILS-ROLS and Operon are typically the most accurate in pure prediction, while PySR offers a strong and stable baseline. LGO variants fall within the competitive envelope: on Cleveland, LGO_{hard} is comparable to Operon in mean R^2 ; on ICU and NHANES, LGOLGO methods span a moderate accuracy range that we later trade for markedly better parsimony and auditable thresholds. The spread of the violins also reveals method stability: Operon and RILS-ROLS show tight dispersions on ICU/NHANES, whereas PSTree displays larger variability. These observations motivate the rest of our analysis: we next examine what LGO learns (thresholds in natural units) and how it uses gates (parsimony) without overfitting.

Primary health datasets: ICU and NHANES

ICU composite risk score (regression). Across 10 random seeds, RILS-ROLS attains the highest accuracy, while LGO_{hard} consistently outperforms LGO_{soft} and is competitive with strong baselines. Table 1 reports mean \pm std on the held-out test set. Concretely, LGO_{hard} reaches $R^2 = 0.800 \pm 0.068$ with $RMSE = 0.817 \pm 0.118$ and $MAE = 0.664 \pm 0.104$, surpassing LGO_{soft} ($R^2 = 0.699 \pm 0.129$). This confirms that explicit (hard) gating better captures the ICU's switch-like dynamics.

Table 1: ICU composite risk score: mean \pm std (10 seeds).

method	experiment	$R^2 \uparrow$	$RMSE \downarrow$	$MAE \downarrow$
PySR	base	0.808 ± 0.028	0.809 ± 0.052	0.656 ± 0.047
PSTree	base	0.504 ± 0.064	1.301 ± 0.078	1.042 ± 0.067
RILS-ROLS	base	0.928 ± 0.029	0.489 ± 0.105	0.342 ± 0.072
Operon	base	0.831 ± 0.026	0.758 ± 0.060	0.614 ± 0.054
LGO	base	0.787 ± 0.093	0.840 ± 0.182	0.673 ± 0.178
LGO	LGO_{soft}	0.699 ± 0.129	0.994 ± 0.216	0.828 ± 0.203
LGO	LGO_{hard}	0.800 ± 0.068	0.817 ± 0.118	0.664 ± 0.104

Performance Comparison

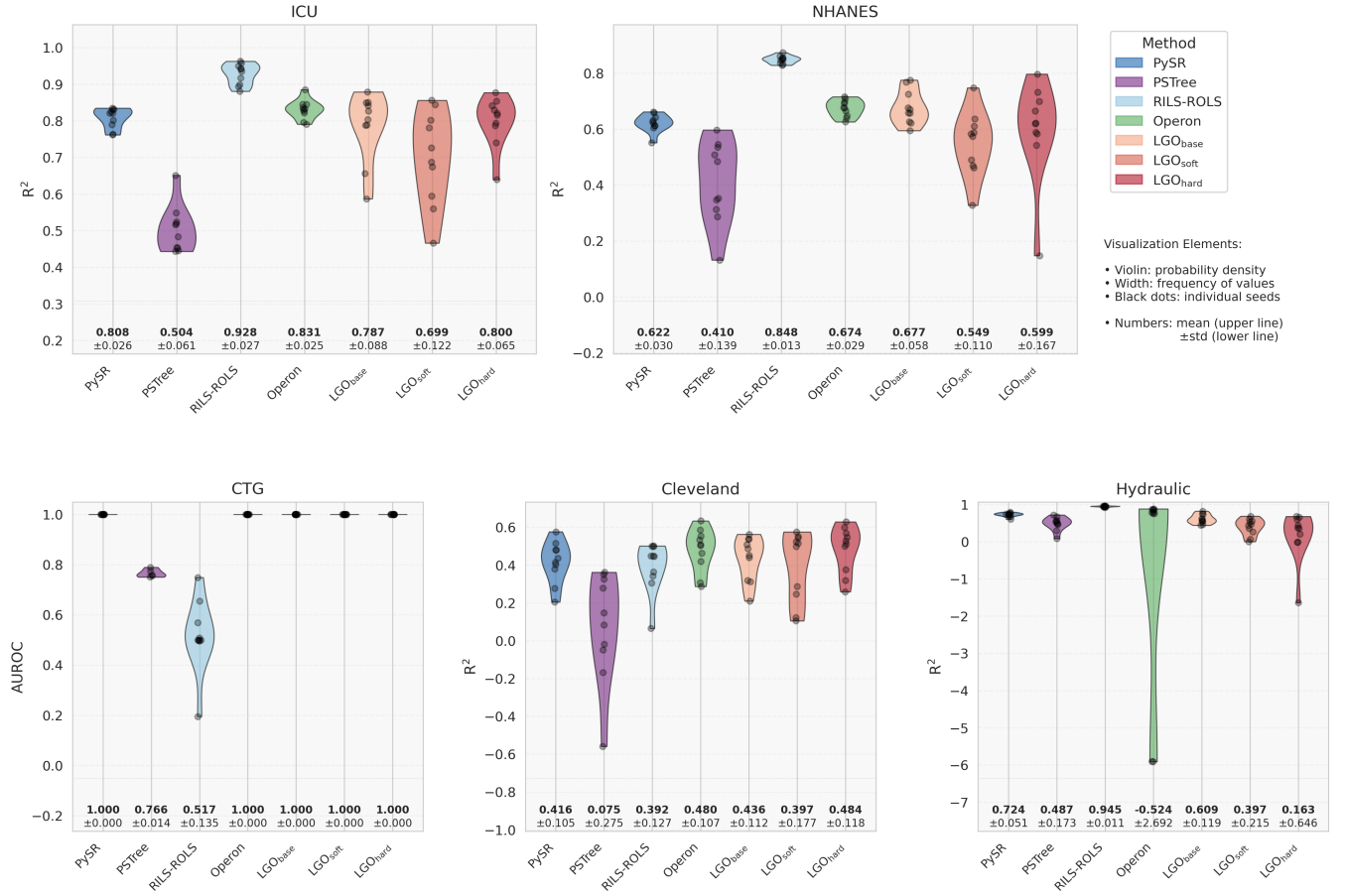


Figure 1: Performance comparison across methods and datasets. Violin plots show the distribution over up to ten seeds per method (Hydraulic excludes 2 anomalous seeds; see SI Table S10). The black dots are individual seeds; violin width reflects probability density. The baseline metric is R^2 for regression datasets and AUROC for CTG; the mean and standard deviation for each violin are printed underneath (mean on the top line, \pm std on the bottom line). The figure provides a high-level accuracy overview before parsimony and interpretability analyses.

NHANES metabolic score (regression). RILS-ROLS again leads in R^2 , followed by Operon, PySR and LGO variants (Table 2). Within LGO, LGO_{hard} ($R^2 = 0.599 \pm 0.176$) remains superior to LGO_{soft} (0.549 ± 0.116), though LGO_{base} is strongest among LGO variants on this dataset (0.677 ± 0.061).

Unit-aware threshold recovery. LGO recovers thresholds in natural units post hoc. For ICU, the LGO_{hard} lactate threshold concentrates around 1.89 mmol/L (IQR [0.79, 2.07]). For NHANES, systolic_bp centers at ~ 128.3 mmHg and fasting glucose at ~ 85.5 mg/dL (Table 3). These values are consistent with the intuition that LGO discovers clinically plausible cutpoints from data.

Table 2: NHANES metabolic score: mean \pm std (10 seeds).

method	experiment	$R^2 \uparrow$	$RMSE \downarrow$	$MAE \downarrow$
PySR	base	0.622 ± 0.031	0.815 ± 0.028	0.660 ± 0.026
PSTree	base	0.410 ± 0.147	1.012 ± 0.119	0.819 ± 0.094
RILS-ROLS	base	0.848 ± 0.014	0.516 ± 0.025	0.404 ± 0.020
Operon	base	0.674 ± 0.030	0.757 ± 0.040	0.604 ± 0.033
LGO	base	0.677 ± 0.061	0.751 ± 0.076	0.600 ± 0.066
LGO	LGO_{soft}	0.549 ± 0.116	0.884 ± 0.107	0.704 ± 0.082
LGO	LGO_{hard}	0.599 ± 0.176	0.828 ± 0.187	0.652 ± 0.140

Table 3: Representative thresholds from LGO_{hard} (median and IQR in natural units).

Feature	Unit	Median	Q1	Q3
ICU lactate	mmol/L	1.886	0.788	2.065
NHANES systolic_bp	mmHg	128.335	128.335	128.895
NHANES fasting_glucose	mg/dL	85.452	74.544	95.400

Threshold interpretability and auditability on ICU and NHANES

We evaluate whether LGO_{hard} discovers clinically meaningful natural-unit thresholds that can be directly audited against domain anchors. For each dataset we retain only features that have both a recovered median threshold and a guideline anchor, and we present the top- k (up to $k = 5$) anchored features for readability. Agreement is quantified by the relative deviation between the LGO median and the anchor (green $\leq 10\%$, yellow $\leq 20\%$, red $> 20\%$). Across all assessable cells, $\approx 71\%$ (5/7) fall within $\leq 10\%$ and 100% within $\leq 20\%$, with no red cells.

On ICU, LGO recovers credible gates for perfusion and hemodynamics: Lactate (mmol/L) and MAP (mmHg) align tightly with anchors, while Respiratory rate (min^{-1}) lies in the yellow band, consistent with a more sensitive monitoring threshold. On NHANES, gates on SBP (mmHg), HDL (mg/dL) and Waist circumference (cm) closely match cardiometabolic anchors (green), and Fasting glucose (mg/dL) indicates an earlier, sensitivity-oriented turning point (yellow). Interquartile ranges (IQR) are narrow for SBP/HDL/Waist, indicating stability of the recovered gates across runs; see Figure 2 for the joint view of agreement and dispersion, and Table 4 for numerical values.

Beyond anchor agreement, we assess the stability of recovered thresholds across the ten random seeds. For each anchored feature we compute the seed-wise median threshold in natural units and summarize dispersion via interquartile ranges (IQR) and a bootstrap 95% CI. Across ICU and NHANES, SBP (mmHg), HDL (mg/dL), and waist circumference (cm) exhibit narrow IQRs, while fasting glucose (mg/dL) shows slightly wider variability yet remains centered in the yellow band relative to the diagnostic anchor — consistent with a conservative, screening-oriented turning point rather than a diagnostic cutoff. These stability views complement Figure 2 and Table 4 by showing not only where the gates land, but how consistently they are recovered across runs. These per-seed medians in Tables 3 and 4 differ from the top- k pool summaries in the SI (Tables S5 – S7), so identical medians/IQRs are not expected across the two views.

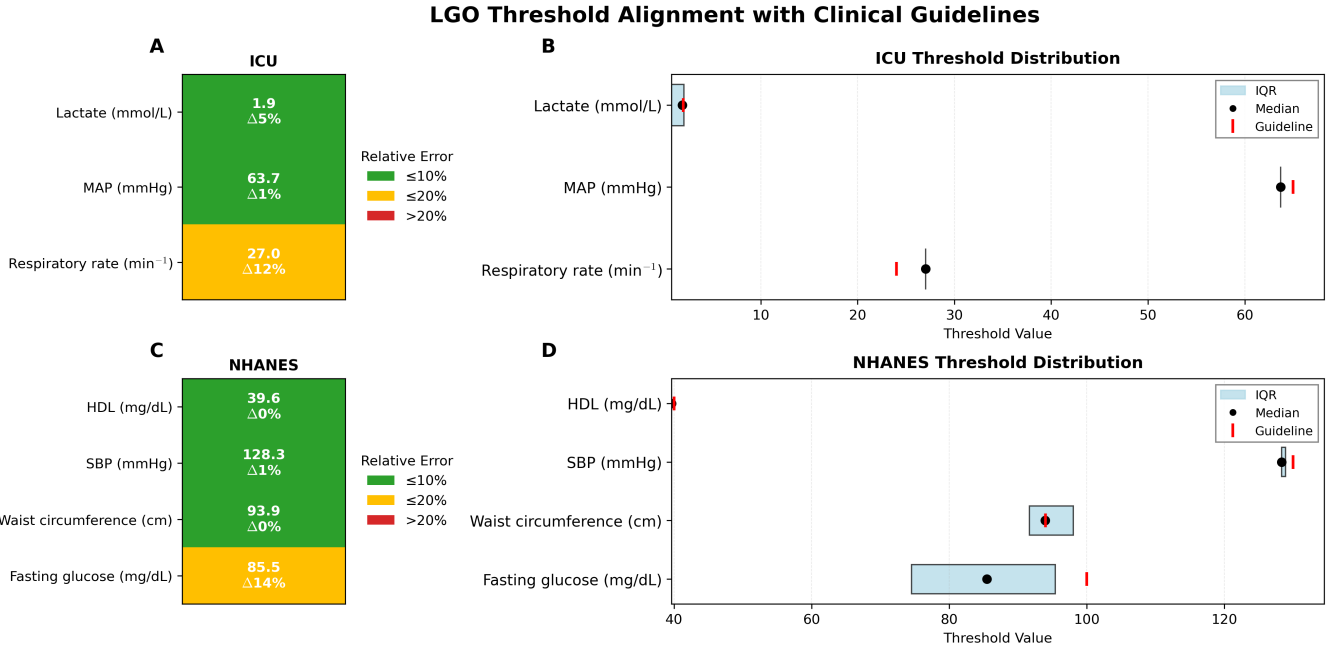


Figure 2: LGO threshold alignment with clinical guidelines (ICU and NHANES). Panels A and C: agreement heatmaps (green $\leq 10\%$, yellow $\leq 20\%$, red $> 20\%$). Only anchored features with valid median thresholds are shown, so grey (N/A) cells are suppressed. Each cell reports the median threshold (natural units) and the relative deviation Δ . Panels B and D: distribution of the same thresholds – horizontal bars show the IQR, black dots mark medians, and red vertical lines mark anchors; the x -axis is in natural units. The figure conveys agreement (A,C) and stability (B,D) without duplicating the numerical details tabulated in Table 4.

Parsimony and gate usage

A key design goal of the LGO family is to express thresholded behavior with as few gates as needed. We therefore quantify parsimony on the top-100 scored models per dataset (ranked by the experiment's objective) along two complementary angles: the fraction of models that contain at least one LGO gate (gate usage %), and the median number of gates per model (zeros included). Together these measures indicate both how often the search relies on a gating mechanism and how many gates it ultimately keeps.

Figure 3 summarizes these measures across datasets and variants. Consistent with our interpretability hypothesis, LGO_{hard} retains a high usage rate where thresholding is truly beneficial (e.g., ICU risk, NHANES metabolic) but prunes gates entirely when the signal does not support them (e.g., in a subset of Cleveland models). When gates are used, LGO_{hard} typically realizes fewer gates per model than LGO_{soft}, yielding a sparser switching structure without sacrificing the ability to form crisp, auditable rules. This pattern aligns with our threshold audit (previous subsection): on ICU, gates for Lactate (mmol/L) and MAP (mmHg) tightly match clinical anchors (green), while Respiratory rate (min^{-1}) lands in the yellow band (27 vs. 24, $\Delta 12\%$), indicating a more sensitive monitor setting rather than a diagnostic cutoff.

Hard gates indeed discover sparser switching structure (Table 5): across datasets the median number of gates is consistently lower for LGO_{hard} than for LGO_{soft} (e.g., ICU: 4.0 vs. 10.0; NHANES: 5.0 vs. 12.5). Combined with the threshold-alignment analysis, these results indicate that LGO_{hard} uses gates selectively and economically — enough to capture clinically/physically meaningful cut-points, yet few enough to keep models compact and auditable.

Table 4: LGO-discovered thresholds (median [Q1, Q3]) versus domain anchors (ICU and NHANES). Values are in natural units.

Dataset	Feature	Median [Q1, Q3]	Anchor	Rel. Err.
ICU	Lactate (mmol/L)	1.89[0.79, 2.07]	2.00	5.70%
ICU	MAP (mmHg)	63.71[63.71, 63.71]	65.00	1.98%
ICU	Respiratory rate (min ⁻¹)	27.04[27.04, 27.04]	24.00	12.66%
NHANES	SBP (mmHg)	128.34[128.34, 128.89]	130.00	1.28%
NHANES	HDL (mg/dL)	39.65[39.65, 39.65]	40.00	0.88%
NHANES	Waist circumference (cm)	93.94[91.67, 98.02]	94.00	0.07%
NHANES	Fasting glucose (mg/dL)	85.45[74.54, 95.40]	100.00	14.55%

Table 5: Gate usage by dataset: median number of gates among top-100 results per dataset.

Dataset	LGO _{soft}	LGO _{hard}
ICU composite risk score	10.0	4.0
NHANES metabolic score	12.5	5.0
UCI CTG NSPbin	12.0	1.0
UCI Heart Cleveland_num	10.0	0.5
UCI HydraulicSys fault score	13.0	3.0

Beyond raw gate counts, the accuracy–complexity trade-off is further illustrated by Pareto fronts (CV loss vs. symbolic complexity). LGO variants occupy favorable regions on ICU and NHANES (lower or comparable CV loss at reduced complexity), consistent with the gate-usage analysis; full fronts for all datasets are provided in Figure S1.

Exemplar symbolic equations

Beyond aggregate statistics, we inspect the top-ranked model per method to visualize what is actually learned. Tables 6 and 7 juxtapose the best equation from LGO_{hard} against strong baselines on ICU and NHANES. Two patterns emerge. First, where thresholds govern the phenomenon (NHANES cardiometabolic risk), LGO_{hard} exposes explicit, unit-aware gates on triglycerides, fasting glucose, SBP, HDL, and waist circumference, aligning with our threshold-audit analysis. Second, when smooth trends suffice (ICU top-1 in this split), LGO_{hard} prunes gates and reduces to smooth primitives — consistent with our parsimony analysis — while baselines also remain smooth and non-auditable. These exemplars complement the gate-usage (Figure 3) and threshold-alignment (Figure 2) results: gates are used selectively, and when used, they yield auditable cut-points in natural units.

Other benchmarks in brief

For completeness, we also evaluated three standard UCI benchmarks. On CTG (binary), Operon, PySR and LGO variants saturate at AUROC/AUPRC ≈ 1.0 , confirming near-separability; PSTree lags and RILS-ROLS underperforms. On Cleveland (regression), LGO_{hard} is competitive with Operon in mean R^2 and yields audit-ready gates on age/cholesterol/thalach (see anchor discussion in the SI). On Hydraulic, relationships are predominantly smooth: RILS-ROLS attains the

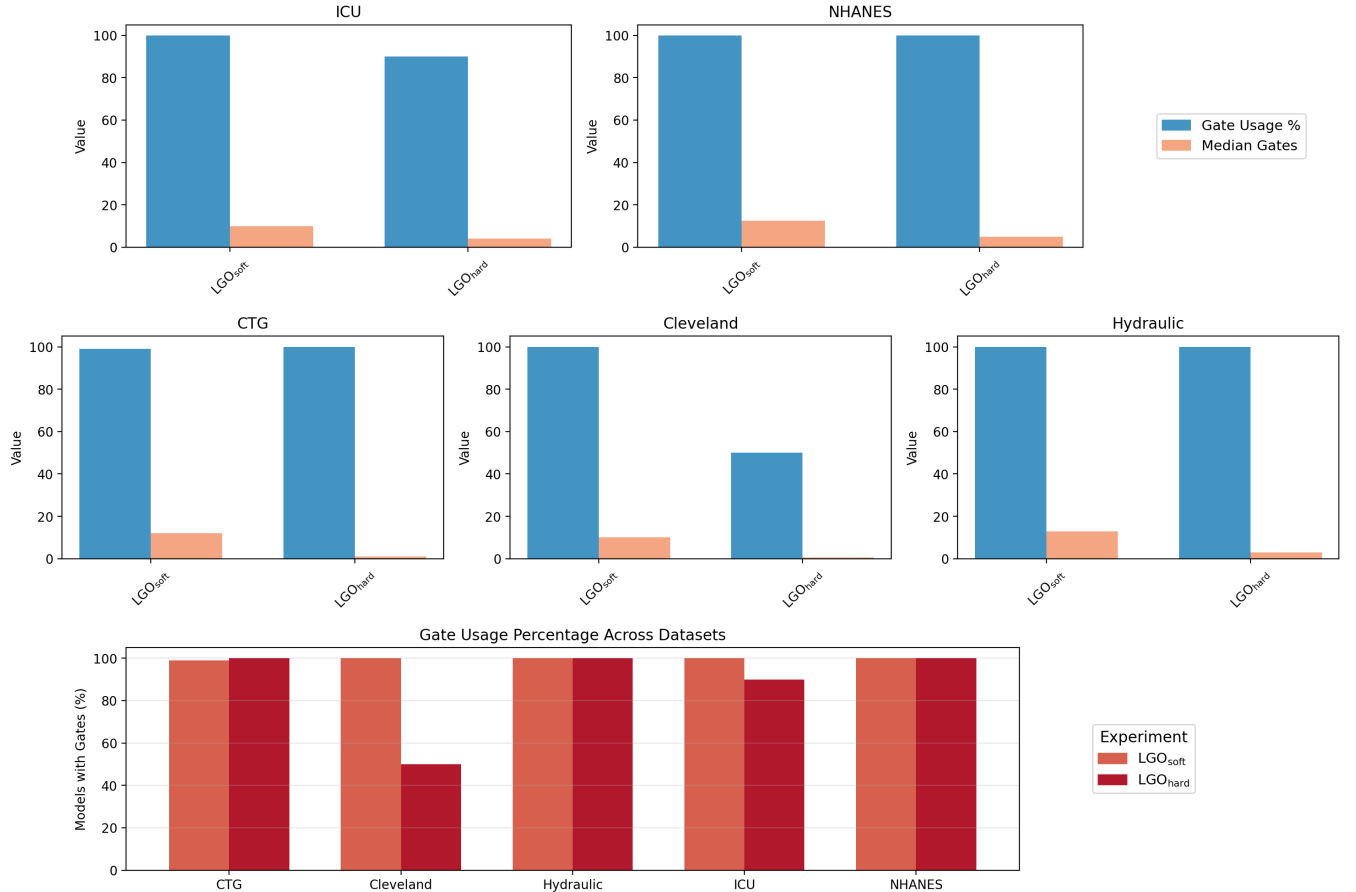


Figure 3: Gating mechanism usage across datasets. Top panels (one subplot per dataset): for LGO_{soft} and LGO_{hard} , the blue bars show gate usage % (fraction of the top-100 models that include at least one LGO gate), and the orange bars show the median number of gates per model (zeros included). Bottom panel: gate usage % aggregated side-by-side across datasets, contrasting LGO_{soft} (light) vs. LGO_{hard} (dark). Hard gates keep usage high where thresholding is needed (ICU, NHANES, CTG) while pruning superfluous gates (e.g., on Cleveland), and they realize fewer gates per model than soft gates, supporting parsimony and auditability.

Table 6: ICU (composite risk): top-1 equations by method (simplified forms for readability).

Method	Experiment	Simplified Expression	Note
LGO	LGO_{hard}	$\hat{y} \approx \alpha_0 + \alpha_1 \sqrt{\text{lactate}} + \alpha_2 \text{vasopressor}$	No explicit gate in top-1 (this split); gates pruned
LGO	LGO _{soft}	nested OR/AND gates over several features	Many gates; less parsimonious
LGO	base	smooth combination of $\sqrt{\text{lactate}}$ and linear terms	No gates by design
PySR	base	$\alpha \text{vasopressor} + \frac{\beta}{\gamma / \sqrt{\text{creatinine} \cdot \text{lactate}^2} + \delta} -$	Smooth surrogate; no explicit thresholds
Operon	base	$\alpha + \beta \sqrt{\text{lactate}} + \gamma \sqrt{\text{vasopressor}}$	Smooth primitives only
RILS-ROLS	base	affine terms + $\exp(\cdot)$ and $\sin(\cdot)$ on lactate/creatinine	Smooth/oscillatory; no thresholds

Table 7: NHANES (metabolic score): top-1 equations by method (simplified forms for readability).

Method	Experiment	Simplified Expression	Note
LGO	LGO_{hard}	$\hat{y} \approx \text{gate}(\text{TG}) + \text{gate}(\text{FG}) + g(\text{SBP}, \text{HDL}, \text{waist})$	Explicit gates (~ 6) on TG, FG, SBP, HDL, waist; thresholds align with anchors (e.g., $\text{TG} \approx 200 \text{ mg/dL}$, $\text{SBP} \approx 128 \text{ mmHg}$)
LGO	LGO _{soft}	many nested gates including gate_expr and OR/AND compositions	Expressive but less parsimonious; more gates than LGO _{hard}
LGO	base	smooth ratios/powers, e.g., $\text{waist}/\text{HDL}, \sqrt{\text{FG} \cdot \text{SBP}}$	No gates by design
PySR	base	$\alpha \frac{\text{waist}}{\text{HDL}} + \beta \sqrt{\text{FG} \cdot \text{SBP}} + \dots$	Compact and smooth; no explicit thresholds
Operon	base	linear combination of waist and triglycerides (plus smooth terms)	Smooth primitives only; no explicit thresholds
RILS-ROLS	base	linear gender term + $\exp(-c_1 \cdot \text{HDL}) + \exp(-c_2 \cdot \text{FG}) + \dots$	Smooth/exponential effects; no explicit thresholds

Reading guide: “gate(x)” denotes a logistic-gated activation on feature x whose threshold is recovered and audited in natural units (see Figure 2); $g(\cdot)$ indicates a smooth subexpression.

Full numeric constants and complete strings appear in the Supplement.

best accuracy, while LGO_{base} remains reasonable and LGO_{hard} underperforms under the fixed budget. Complete mean \pm std tables and per-dataset Pareto fronts are reported in Tables S8–S10 and Figure S1.

Ablation within the LGO family

To isolate LGO components, we compare three operator sets inside the same engine: base (no gates), LGO_{soft}, and LGO_{hard}. Table 8 summarizes R^2 medians (IQR) over 10 seeds. LGO_{hard} outperforms LGO_{soft} on ICU and Cleveland, and is closer to (or slightly above) base on threshold-heavy tasks; on Hydraulic, introducing hard gates can hurt when relations are predominantly smooth.

Table 8: Ablation within LGO: medians (IQR) of R^2 over 10 seeds.

Dataset	Base	LGO _{soft}	LGO _{hard}
ICU composite risk score	0.815 (0.059)	0.706 (0.182)	0.818 (0.049)
NHANES metabolic score	0.664 (0.079)	0.579 (0.130)	0.621 (0.106)
UCI Heart Cleveland num	0.469 (0.180)	0.506 (0.282)	0.520 (0.157)
UCI HydraulicSys fault score	0.586 (0.168)	0.450 (0.264)	0.367 (0.516)

Discussion

From readable formulas to auditable thresholds

Symbolic regression (SR) is often positioned as a route to readable models, but readability alone is not sufficient for scientific and regulatory practice^{3,4,19}. In high-stakes domains, stakeholders ask more pointed questions: Where is the decision boundary? In what physical units? Does it agree with domain guidelines? The Logistic-Gated Operator (LGO) family proposed here operationalizes these requirements by making thresholds first-class citizens in the SR search. Instead of relying on long arithmetic compositions to approximate step-like behavior, LGO provides gating primitives with learnable location and steepness that are trained in standardized space and audited back in natural units. This yields what we call executable interpretability: the model encodes not only a compact algebraic form, but also explicit, unit-aware cut-points that can be checked against clinical or engineering anchors.

Agreement with domain anchors (Figure 2; Table4) substantiates this claim. On ICU and NHANES, $\approx 71\%$ (5/7) of assessed gates fall within $\leq 10\%$ and 100% within $\leq 20\%$ of guideline thresholds in natural units, with no red cells. The ICU gates for Lactate (mmol/L) and MAP (mmHg) align tightly with Sepsis/critical-care anchors (2.0 mmol/L and 65 mmHg, respectively)^{7,8}, while NHANES gates concur with cardiometabolic anchors for SBP, HDL and waist circumference^{9–11}. The fasting-glucose gate appears earlier than the diagnostic cutoff (yellow band), surfacing a conservative, sensitivity-oriented turning point — useful for screening workflows.

Parsimony of gating (Figure 3; Table5) provides a second line of evidence. Across datasets, LGO_{hard} uses fewer gates per model than LGO_{soft} (e.g., ICU 4.0 vs 10.0; NHANES 5.0 vs 12.5 median gates among top-100 models), while maintaining high usage rates only where thresholding is supported by data. This selective economy is consistent with our ablations (Table 8): hard gates outperform or match soft gates on threshold-heavy problems (ICU, Cleveland), and are near base on smoother tasks.

A third perspective is competitive accuracy with distributional stability (Figure 1). Although our goal is not to chase SOTA point estimates, LGO sits within the competitive envelope across datasets relative to strong SR baselines (RILS-ROLS, Operon, PySR). The violins reveal reasonable dispersion across seeds, and when a small loss in pure accuracy occurs, it is compensated by the gains in auditability and sparsity — a trade-off explicitly desired in scientific and clinical modeling³.

Together, these findings indicate that LGO turns interpretability from a post-hoc explanation problem into a first-class modeling constraint: we search directly in a space where threshold structure is easy to express, easy to audit, and easy to communicate.

Methodological significance within symbolic regression

Classical GP-based SR evolves programs over arithmetic and elementary functions^{1,2}. Recent systems (e.g., AI-Feynman, PySR) improved efficiency and discovery quality via physics-inspired priors, equation simplification and mixed search strategies^{24,27,29}. LGO complements this line by re-designing the primitive set: we add logistic gates — with differentiable parameters (a, b) — to make piecewise behavior natively representable and tunable. This design is informed by decades of gating in neural networks (e.g., LSTM/GRU, mixture-of-experts)^{36–38}, but transplanted into SR where gates are symbolic nodes and their parameters are audited back to physical units.

A unit-aware standardize-and-invert pipeline is central to this design. All features are standardized (z-scores) for stable search, and learned thresholds are inverted with train-only statistics to natural units. This resolves the common pitfall where predictions are compared across mismatched scales; we also add self-checks ($\text{RMSE} \geq \text{MAE}$, internal vs external agreement, anomaly scans) to guard against silent failure modes.

A complementary choice concerns hard versus soft gating. LGO_{hard} (threshold gate) and LGO_{soft} (multiplicative gate) realize different inductive biases: hard gates favor sparse switching (few gates, crisp regimes), whereas soft gates favor graded modulation. Our data show that LGO_{hard} better matches anchor-driven tasks (ICU/NHANES), whereas on globally smooth dynamics (Hydraulic) adding gates may not help — consistent with the view that the primitive set should reflect the system's mechanism.

This perspective — curating mechanism-aware primitives — is general. Beyond thresholds, one can introduce periodic or saturation operators with parameters that audit back to natural units (e.g., period in seconds, saturation level in mmol/L), closing the loop between data-fit and domain semantics.

Clinical and engineering impact: from numbers to rules

Because LGO thresholds are explicitly mapped to natural units, audit becomes an arithmetic operation: compare a recovered cut-point to its guideline anchor and read off the deviation. In ICU, clinicians can verify that $\text{MAP} = 63.7 \text{ mmHg}$ and $\text{lactate} = 1.89 \text{ mmol/L}$ are sensible escalation gates; in NHANES, SBP at 128.3 mmHg , HDL at 39.65 mg/dL , and waist circumference at 93.94 cm align with cardiometabolic anchors, while fasting glucose around 85.5 mg/dL surfaces an earlier turning point suitable for screening rather than diagnosis. This alignment supports clinical review, protocol integration, and post-deployment monitoring, and it translates model outputs into unit-aware rules that stakeholders can directly discuss^{5,6}.

From an engineering standpoint, gates formalize operating envelopes. A symbolic form like $f(x) \sigma(a(f(x) - b))$ exposes both the algebra and the trip point b , so teams can wire dashboards, alarms, and acceptance tests directly to the recovered threshold in physical units. When guidance evolves (e.g., hypertension tiers), the same audit can be re-run by updating anchors; deviations then quantify how far the data-driven rule drifts from the new consensus. In this sense, LGO operationalizes a governance-ready loop: readable equations, unit-aware thresholds, and low-friction re-audits as standards change.

Interpreting “yellow” cells: screening versus diagnosis

Yellow-band deviations (e.g., fasting glucose in NHANES; Figure 2C) are best read as earlier change-points rather than errors. For risk stratification and routine monitoring, a conservative turning point can be preferable to a diagnostic cutoff: the former flags emerging risk, while the latter certifies disease. We therefore explicitly separate screening-appropriate gates — often earlier and yellow — from diagnostic thresholds—typically green—so that model interpretation follows clinical workflow.

Dimensional consistency and anchor curation

Auditing in natural units presupposes dimensional consistency. We standardize all continuous features in z -space for stable search and then invert thresholds with train-only statistics; anchors are curated with explicit units and documented sources. We avoid constant anchors for variables whose reference levels depend on age or context (e.g., counts or age-indexed normals) and record exclusions in the guideline catalogue. Looking ahead, typed semantics could be extended with physical-dimension types, further constraining operator compositions to unit-consistent forms and tightening the audit loop.

Failure modes and limitations

When relations are globally smooth, adding gates can over-parameterize. On Hydraulic, trends are largely smooth and arithmetic-only SR or gradient-aided variants can dominate; this supports a mechanism-selection view in which LGO is preferred when regime switching is plausible, and smooth primitives otherwise.

Anchor validity matters. Some features (e.g., thalach or categorical counts in Cleveland) do not admit a single constant anchor; a yellow or red cell in such cases often reflects anchor mis-specification rather than model error. Our pipeline therefore filters categorical/count features out of anchor-based scoring and documents curation decisions.

Computation is a practical constraint. Searching over (a, b) introduces continuous parameters; we mitigate the overhead with typed search, local refinements, and early self-checks, but budgets still matter relative to arithmetic-only SR.

Finally, **aggregate versus per-seed coverage can differ.** The main text reports medians and IQRs for thresholds across runs; per-seed coverage (how often a gate appears) is supported by our tooling and can be reproduced from the released scripts when full per-seed exports are available.

Guidance for practitioners

When to use LGO. Choose LGO when domain knowledge suggests regime switching — alerts, safety limits, or phase changes. Begin with LGO_{hard} to encourage parsimonious, auditable rules, and fall back to LGO_{soft} when graded modulation is expected.

Curation and configuration. Curate anchors with clear consensus and units (e.g., MAP 65 mmHg; HDL 40 mg/dL), and avoid constant anchors for categorical/count features or age-indexed normals. For search, increase budget when gates are rare; enable `gate_expr` to gate sub-expressions; keep z -score scaling with train-only statistics; always invert thresholds to natural units for evaluation.

Audit and deployment. Report medians and IQRs of thresholds, $\text{mean} \pm \text{std}$ of metrics, and the traffic-light deviations against anchors; use self-checks ($\text{RMSE} \geq \text{MAE}$, internal vs. external RMSE, anomaly scans) and state explicitly whether a gate is intended for screening or for diagnosis. For deployment, export gates as unit-aware rules with readable names and units, connect dashboards/alarms to b_{raw} , and maintain a changelog when anchors or units are updated.

Broader outlook

LGO reframes SR as mechanism-aware program synthesis. By elevating thresholds to primitives with auditable parameters, we close the loop between equation discovery and domain governance. The same recipe can be extended to periodic (e.g., $\sin(2\pi t/T)$ with period T in seconds), saturation (Michaelis-Menten with K_m in mmol/L), or dose-response gates, each parameterizing a scientifically meaningful quantity.

We also see opportunities in uncertainty-aware LGO that reports bootstrap credible intervals for b , in subgroup-aware audits that assess fairness across age/sex/ethnicity in NHANES, in temporal LGO tailored to ICU time-series, and in mechanistic hybrids that constrain gates by physics/physiology priors^{30,43}. Rather than competing solely on black-box accuracy, we advocate a standards-aligned path where models expose the levers that matter to practitioners.

Experimental procedures

Resource availability

Lead contact

Requests for further information and resources should be directed to and will be fulfilled by the lead contact, Ou Deng (dengou@toki.waseda.jp).

Materials availability

This study did not generate new unique reagents.

Data and code availability

All datasets are public: MIMIC-IV¹⁴ (de-identified; data use agreement required), NHANES¹⁷ (CDC public release), and UCI repositories (CTG⁴⁹, Cleveland⁵⁰, Hydraulic⁵¹). The repository provides download pointers and preprocessing scripts. No identifiable personal information is included in released artifacts. Thresholds are reported in natural units for scientific audit only and are not intended for clinical use without prospective validation.

All code to reproduce results (LGO primitives; typed GP engine; baselines PySR, Operon, PSTree, RILS-ROLS; plotting and aggregation scripts) is available on GitHub: <https://github.com/oudeng/LGO>. A camera-ready snapshot will be archived on Zenodo (DOI: 10.5281/zenodo.17299423). Reproducibility details (software environments, artifact index, operator sets/budgets) are summarized in SI §1; Tables S1–S3.

Overview of experimental workflow

To make the end-to-end protocol explicit without duplicating SI, we summarize the workflow as follows:

1. **Data access and preprocessing.** Download public datasets and apply the repository’s preprocessing to obtain feature matrices/targets; continuous features are standardized to z -scores using *training-only* statistics.
2. **Typed SR configuration.** Instantiate a strongly typed GP (STGP) with the LGO primitive family and typed domains Feat/Pos/Thr. We study three operator sets: base (no gates), LGO_{soft} (magnitude-preserving), and LGO_{hard} (logistic gate).
3. **Population search.** Run tournament selection with subtree crossover/mutation; enable a micro-mutation on each LGO node to perturb gate parameters (a, b) locally.
4. **Model selection and refit.** Maintain Pareto pools under a cross-validation (CV) proxy during search, then refit the selected candidates on the training split; finally apply local coordinate descent on (a, b) while keeping structure fixed.
5. **Threshold inversion and audit.** Map learned thresholds from z -space to natural units via training-only (μ, σ) , compare with curated anchors in config/guidelines.yaml, and compute traffic-light deviations (green $\leq 10\%$, yellow $\leq 20\%$, red $> 20\%$).
6. **Reporting and exports.** Report mean \pm std over ten seeds on the test split; export per-seed metrics, expressions, gate counts, and candidate pools for reproducibility. Extended Pareto fronts appear in Figure S1; UCI benchmark tables are S8–S10.

LGO-SR framework: typed GP with unit-aware gates

We embed Logistic-Gated Operators (LGO) into a strongly typed GP (STGP) pipeline implemented atop DEAP’s gp module⁶⁴, following typed GP principles²². The type system separates feature values (Feat), positive steepness parameters (Pos), and threshold parameters (Thr). Pos is enforced via a softplus reparameterization; Thr is bounded in standardized (z -score) space to stabilize search. We consider three operator configurations: base (no gates), LGO_{soft} (magnitude-preserving gates), and LGO_{hard} (pure logistic gates). Evolution runs entirely in standardized space; after training, learned thresholds are mapped back to natural units with training-only statistics, enabling unit-aware audit. Formal operator definitions, gradients used in local refinements, and the standardize-and-invert recipe appear in the SI §2.

Search, model selection, and local refinement

Population-based search uses tournament selection with subtree crossover/mutation and a targeted micro-mutation that perturbs each LGO node’s (a, b) to refine location and steepness. A cross-validation proxy is monitored during evolution to rank candidates and form Pareto pools (accuracy–complexity); selected programs are refit on the training split, after which we run a local coordinate descent on (a, b) with fixed structure. Unified budgets (population, generations), typed operator sets, micro-mutation probabilities, and CV-proxy settings are consolidated in SI Table S3; the public artifact index (entry script, configs, anchors) is listed in SI Table S2.

Baselines and fair comparison

We compare against representative SR engines with public implementations and active community use: PySR²⁷, Operon²⁵, PSTree²⁶, and RILS–ROLS²⁸. Budgets and operator sets are aligned

across engines where applicable; engine-specific options (e.g., complexity penalties, search-space toggles) follow the repository defaults and are recorded in SI Tables S2–S3. All metrics (RMSE, MAE, R^2 ; AUROC/AUPRC/Brier for CTG) are computed from the same (y, \hat{y}) pairs with seed-wise reporting; self-checks (RMSE \geq MAE, internal vs. external metric consistency, anomaly scans) are enforced and described in SI §1 (Self-checks and exports).

Threshold recovery and audit

For each gated feature or gated sub-expression, the learned threshold in standardized space is converted to natural units using training-only statistics and compared with dataset-specific anchors curated in `config/guidelines.yaml`. Agreement is quantified as relative deviation with traffic-light bands (green $\leq 10\%$, yellow $\leq 20\%$, red $> 20\%$). Aggregation scripts compute per-feature medians and IQRs and generate the threshold-alignment plots in the main text. The anchor schema, provenance, and audit procedure are detailed in SI §4; comprehensive threshold summaries for ICU and NHANES appear in Tables S6–S7, and gate-usage statistics for top- k candidates are in Table S5.

Statistical reporting

Unless stated otherwise, we report the mean \pm standard deviation across ten random seeds on a held-out test split (regression: R^2 , RMSE, MAE; CTG: AUROC, AUPRC, Brier). Threshold summaries report medians with interquartile ranges. Extended Pareto fronts (CV loss vs. symbolic complexity) are shown in SI Figure S1. Full per-seed exports (metrics, expressions, gate counts, Pareto pools) are included in the public artifact indexed in SI Table S2; canonical rewrite rules used for expression simplification are listed in SI Table S4; top- k gate-usage and threshold tables are SI Tables S5–S7; and UCI benchmark summaries are SI Tables S8–S10.

Acknowledgments

The work was supported in part by the 2022-2024 Masaru Ibuka Foundation Research Project on Oriental Medicine, 2020-2025 JSPS A3 Foresight Program (Grant No. JPJSA3F20200001), 2022-2024 Japan National Initiative Promotion Grant for Digital Rural City, 2023 and 2024 Waseda University Grants for Special Research Projects (Nos. 2023C-216 and 2024C-223), 2023-2024 Waseda University Advanced Research Center Project for Regional Cooperation Support, and 2023-2024 Japan Association for the Advancement of Medical Equipment (JAAME) Grant.

Author contributions

Conceptualization: O.D. Methodology: O.D. Software: O.D. Hardware: O.D., S.N. Datasets: R.C., J.X., O.D. Validation: O.D., R.C. Formal Analysis: O.D. Investigation: O.D. Writing – Original Draft: O.D. Writing – Review & Editing: R.C., S.N., A.O., Q.J. Visualization: O.D., R.C. Supervision: S.N., A.O., Q.J. Funding Acquisition: S.N., A.O., Q.J.

Declaration of interests

The authors declare no competing interests.

References

1. Koza, J. R. (1994). Genetic programming as a means for programming computers by natural selection. *Statistics and Computing* 4, 87–112. doi:10.1007/BF00175355.
2. Schmidt, M., and Lipson, H. (2009). Distilling free-form natural laws from experimental data. *Science* 324, 81–85. doi:10.1126/science.1165893.
3. Rudin, C. (2019). Stop explaining black box machine learning models for high stakes decisions and use interpretable models instead. *Nature Machine Intelligence* 1, 206–215. doi:10.1038/s42256-019-0048-x.
4. Molnar, C. *Interpretable Machine Learning*. 3 ed. (2025). ISBN 978-3-911578-03-5. URL: <https://christophm.github.io/interpretable-ml-book> accessed: 2025-09-22.
5. Wiens, J., Saria, S., Sendak, M., and et al. (2019). Do no harm: A roadmap for responsible machine learning for health care. *Nature Medicine* 25, 1337–1340. doi:10.1038/s41591-019-0548-6.
6. Topol, E. J. (2019). High-performance medicine: The convergence of human and artificial intelligence. *Nature Medicine* 25, 44–56. doi:10.1038/s41591-018-0300-7.
7. Singer, M., Deutschman, C. S., Seymour, C. W., and et al. (2016). The third international consensus definitions for sepsis and septic shock (sepsis-3). *JAMA* 315, 801–810. doi:10.1001/jama.2016.0287.
8. Rhodes, A., Evans, L. E., Alhazzani, W., and et al. (2017). Surviving sepsis campaign: International guidelines for management of sepsis and septic shock: 2016. *Intensive Care Medicine* 43, 304–377. doi:10.1007/s00134-017-4683-6.
9. Whelton, P. K., Carey, R. M., Aronow, W. S., and et al. (2018). 2017 acc/aha/abc/acpm/ags/apha/ash/aspc/nma/pcna guideline for the prevention, detection, evaluation, and management of high blood pressure in adults: A report of the american college of cardiology/american heart association task force on clinical practice guidelines. *Hypertension* 71, e13–e115. doi:10.1161/HYP.0000000000000065.
10. Grundy, S. M., Stone, N. J., Bailey, A. L., and et al. (2019). 2018 aha/acc/aacvpr/aapa/abc/acpm/ada/ags/apha/aspc/nla/pcna guideline on the management of blood cholesterol: A report of the american college of cardiology/american heart association task force on clinical practice guidelines. *Circulation* 139, e1082–e1143. doi:10.1161/CIR.0000000000000625.
11. Alberti, K. G. M. M., Zimmet, P., and Shaw, J. (2006). Metabolic syndrome—a new worldwide definition. a consensus statement from the international diabetes federation. *Diabetic Medicine* 23, 469–480. doi:10.1111/j.1464-5491.2006.01858.x.

12. ElSayed, N. A., Aleppo, G., Aroda, V. R., and et al. on behalf of the American Diabetes Association (2023). 2. classification and diagnosis of diabetes: Standards of care in diabetes—2023. *Diabetes Care* *46*, S19–S40. doi:10.2337/dc23-S002.
13. U.S. Food and Drug Administration, Health Canada, and Medicines and Healthcare products Regulatory Agency. Good machine learning practice for medical device development: Guiding principles. Guidance Document U.S. Food and Drug Administration (2021). URL: <https://www.fda.gov/medical-devices/software-medical-device-samd/good-machine-learning-practice-medical-device-development-guiding-principles> joint publication by FDA, Health Canada, and UK MHRA. Accessed: 2025-9-22.
14. Johnson, A. E. W., Bulgarelli, L., Shen, L., Gayles, A., and et al. (2023). Mimic-iv, a freely accessible electronic health record dataset. *Scientific Data* *10*, 1. doi:10.1038/s41597-022-01899-x.
15. Johnson, A., Bulgarelli, L., Pollard, T., and et al. (2024). MIMIC-IV (version 3.1). PhysioNet. doi:10.13026/kpb9-mt58.
16. Goldberger, A., Amaral, L., Glass, L., and et al. (2000). PhysioBank, PhysioToolkit, and PhysioNet: Components of a new research resource for complex physiologic signals. *Circulation* *101*, e215–e220. [Online]. RRID:SCR_007345.
17. Stierman, B., Afful, J., Carroll, M. D., and et al. (2021). National health and nutrition examination survey 2017–march 2020 prepandemic data files—development of files and prevalence estimates for selected health outcomes. *National Health Statistics Reports*. doi:10.15620/cdc:106273.
18. on behalf of the European Diabetes Epidemiology Group, D. S. G. (2001). Glucose tolerance and cardiovascular mortality: Comparison of fasting and 2-hour diagnostic criteria. *Archives of Internal Medicine* *161*, 397–405. doi:10.1001/archinte.161.3.397.
19. Lipton, Z. C. (2018). The mythos of model interpretability. *Communications of the ACM* *61*, 36–43. doi:10.1145/3233231.
20. Banzhaf, W., Francone, F. D., Keller, R. E., and Nordin, P. Genetic programming: an introduction: on the automatic evolution of computer programs and its applications. Morgan Kaufmann Publishers Inc. (1998). ISBN 155860510X. URL: <https://dl.acm.org/doi/book/10.5555/280485> accessed: 2025-09-22.
21. Poli, R., Langdon, W. B., and McPhee, N. F. A Field Guide to Genetic Programming. Lulu Enterprises, UK Ltd (2008). ISBN 1409200736. URL: <https://dl.acm.org/doi/10.5555/1796422> accessed: 2025-09-22.
22. Montana, D. J. (1995). Strongly typed genetic programming. *Evolutionary Computation* *3*, 199–230. doi:10.1162/evco.1995.3.2.199.
23. La Cava, W., Spector, L., and Danai, K. (2016). Epsilon-lexicase selection for regression. In: *Proceedings of the Genetic and Evolutionary Computation Conference 2016. GECCO '16* (741–748). doi:10.1145/2908812.2908898.
24. La Cava, W., Burlacu, B., Virgolin, M., and et al. (2021). Contemporary symbolic regression methods and their relative performance. *Adv Neural Inf Process Syst* *2021*, 1–16. URL: <https://pmc.ncbi.nlm.nih.gov/articles/PMC11074949/>. Accessed: 2025-9-22.

25. Burlacu, B., Kronberger, G., and Kommenda, M. (2020). Operon c++: an efficient genetic programming framework for symbolic regression. In: Proceedings of the 2020 Genetic and Evolutionary Computation Conference Companion. GECCO '20 (1562–1570). doi:10.1145/3377929.3398099.
26. Zhang, H., Zhou, A., Qian, H., and Zhang, H. (2022). Ps-tree: A piecewise symbolic regression tree. *Swarm and Evolutionary Computation* 71, 101061. doi:<https://doi.org/10.1016/j.swevo.2022.101061>.
27. Cranmer, M. (2023). Interpretable machine learning for science with pysr and symbolicregression.jl. arXiv:2305.01582.
28. Kartelj, A., and Djukanović, M. (2023). Rils-rols: robust symbolic regression via iterated local search and ordinary least squares. *Journal of Big Data* 10, 71. doi:10.1186/s40537-023-00743-2.
29. Udrescu, S.-M., and Tegmark, M. (2020). Ai feynman: A physics-inspired method for symbolic regression. *Science Advances* 6, eaay2631. doi:10.1126/sciadv.aay2631.
30. Cranmer, M., Sanchez-Gonzalez, A., Battaglia, P., and et al. (2020). Discovering symbolic models from deep learning with inductive biases. In: Proceedings of the 34th International Conference on Neural Information Processing Systems. (NIPS '20). URL: <https://dl.acm.org/doi/10.5555/3495724.3497186> accessed: 2025-9-22.
31. Petersen, B. K., Larma, M. L., Mundhenk, T. N., and et al. (2021). Deep symbolic regression: Recovering mathematical expressions from data via risk-seeking policy gradients. In: International Conference on Learning Representations. (ICLR 2021 Oral). URL: <https://openreview.net/forum?id=m5Qsh0kBQG> accessed: 2025-9-22.
32. Kim, S., Lu, P. Y., Mukherjee, S., and et al. (2021). Integration of neural network-based symbolic regression in deep learning for scientific discovery. *IEEE Transactions on Neural Networks and Learning Systems* 32, 4166–4177. doi:10.1109/TNNLS.2020.3017010.
33. Kusner, M. J., Paige, B., and Hernández-Lobato, J. M. (2017). Grammar variational autoencoder. In: Proceedings of the 34th International Conference on Machine Learning vol. 70 of *ICML'17*. (1945–1954). URL: <https://dl.acm.org/doi/10.5555/3305381.3305582> accessed: 2025-9-22.
34. Sahoo, S., Lampert, C., and Martius, G. (2018). Learning equations for extrapolation and control. In: Proceedings of the 35th International Conference on Machine Learning vol. 80 of *PMLR*. (4442–4450). URL: <http://proceedings.mlr.press/v80/sahoo18a/sahoo18a.pdf> accessed: 2025-9-22.
35. Liu, H., Simonyan, K., and Yang, Y. (2019). DARTS: Differentiable architecture search. In: International Conference on Learning Representations. (ICLR). URL: <https://openreview.net/forum?id=S1eYHoC5FX> accessed: 2025-9-22.
36. Hochreiter, S., and Schmidhuber, J. (1997). Long short-term memory. *Neural Computation* 9, 1735–1780. doi:10.1162/neco.1997.9.8.1735.
37. Cho, K., van Merriënboer, B., Gulcehre, C., and et al. (2014). Learning phrase representations using rnn encoder–decoder for statistical machine translation. In: Proceedings of the 2014 Conference on Empirical Methods in Natural Language Processing (EMNLP). (1724–1734). doi:10.3115/v1/D14-1179.

38. Jacobs, R. A., Jordan, M. I., Nowlan, S. J., and Hinton, G. E. (1991). Adaptive mixtures of local experts. *Neural Computation* *3*, 79–87. doi:10.1162/neco.1991.3.1.79.

39. Montúfar, G., Pascanu, R., Cho, K., and Bengio, Y. (2014). On the number of linear regions of deep neural networks. In: *Proceedings of the 28th International Conference on Neural Information Processing Systems* vol. 2 of *NIPS '14*. (2924–2932). URL: <https://dl.acm.org/doi/10.5555/2969033.2969153> accessed: 2025-9-22.

40. Letham, B., Rudin, C., McCormick, T. H., and Madigan, D. (2015). Interpretable classifiers using rules and bayesian analysis: Building a better stroke prediction model. *The Annals of Applied Statistics* *9*, 1350–1371. doi:10.1214/15-AOAS848.

41. Frosst, N., and Hinton, G. (2017). Distilling a neural network into a soft decision tree. *arXiv*:1711.09784.

42. Kortschieder, P., Fiterau, M., Criminisi, A., and Bulò, S. R. (2015). Deep neural decision forests. In: *2015 IEEE International Conference on Computer Vision (ICCV)*. (1467–1475). doi:10.1109/ICCV.2015.172.

43. Brunton, S. L., Proctor, J. L., and Kutz, J. N. (2016). Discovering governing equations from data by sparse identification of nonlinear dynamical systems. *Proceedings of the National Academy of Sciences* *113*, 3932–3937. doi:10.1073/pnas.1517384113.

44. Raissi, M., Perdikaris, P., and Karniadakis, G. E. (2019). Physics-informed neural networks: A deep learning framework for solving forward and inverse problems involving nonlinear partial differential equations. *Journal of Computational Physics* *378*, 686–707. doi:10.1016/j.jcp.2018.10.045.

45. Lu, L., Jin, P., Pang, G., and et al. (2021). Learning nonlinear operators via deeponet based on the universal approximation theorem of operators. *Nature Machine Intelligence* *3*, 218–229. doi:10.1038/s42256-021-00302-5.

46. Li, Z., Kovachki, N. B., Azizzadenesheli, K., and et al. (2021). Fourier neural operator for parametric partial differential equations. In: *International Conference on Learning Representations*. (ICML). URL: <https://openreview.net/forum?id=c8P9NQVtmn0> accessed: 2025-9-22.

47. Villar, S., Hogg, D. W., Storey-Fisher, K., Yao, W., and Blum-Smith, B. (2021). Scalars are universal: equivariant machine learning, structured like classical physics. In: *Proceedings of the 35th International Conference on Neural Information Processing Systems*. (NIPS '21). URL: <https://dl.acm.org/doi/10.5555/3540261.3542471> accessed: 2025-9-22.

48. Batzner, S., Musaelian, A., Sun, L., and et al. (2022). E(3)-equivariant graph neural networks for data-efficient and accurate interatomic potentials. *Nature Communications* *13*, 2453. doi:10.1038/s41467-022-29939-5.

49. Campos, D., and Bernardes, J. (2000). Cardiotocography. UCI Machine Learning Repository. doi:10.24432/C51S4N.

50. Janosi, A., Steinbrunn, W., Pfisterer, M., and Detrano, R. (1989). Heart Disease. UCI Machine Learning Repository. doi:10.24432/C52P4X.

51. Helwig, N., Pignanelli, E., and Schtze, A. (2015). Condition monitoring of hydraulic systems. UCI Machine Learning Repository. doi:10.24432/C5CW21.

52. Sobolá, I. M. (2001). Global sensitivity indices for nonlinear mathematical models and their monte carlo estimates. *Mathematics and Computers in Simulation* *55*, 271–280. doi:10.1016/S0378-4754(00)00270-6.

53. Herman, J., and Usher, W. (2017). Salib: An open-source python library for sensitivity analysis. *Journal of Open Source Software* *2*, 97. doi:10.21105/joss.00097.

54. Glymour, C., Zhang, K., and Spirtes, P. (2019). Review of causal discovery methods based on graphical models. *Frontiers in Genetics* *10*, 524. doi:10.3389/fgene.2019.00524.

55. Rubin, D. B. (1976). Inference and missing data. *Biometrika* *63*, 581–592. doi:10.1093/biomet/63.3.581.

56. Shimizu, S., Inazumi, T., Sogawa, Y., and et al. (2011). Directlingam: A direct method for learning a linear non-gaussian structural equation model. *Journal of Machine Learning Research* *12*, 1225–1248. URL: <https://dl.acm.org/doi/10.5555/1953048.2021040>. Accessed: 2025-9-22.

57. Grayeli, A., Sehgal, A., Costilla-Reyes, O., and et al. (2025). Symbolic regression with a learned concept library. In: Proceedings of the 38th International Conference on Neural Information Processing Systems. (NIPS '24). URL: <https://dl.acm.org/doi/10.5555/3737916.3739335> accessed: 2025-9-2.

58. Tian, Y., Zhou, W., Viscione, M., and et al. (2025). Interactive symbolic regression with co-design mechanism through offline reinforcement learning. *Nature Communications* *16*, 3930. doi:10.1038/s41467-025-59288-y.

59. Raghav, S. S., Kumar, S. T., Balaji, R., Sanjay, M., and Shunmuga, C. (2024). Interactive symbolic regression - a study on noise sensitivity and extrapolation accuracy. In: Proceedings of the Genetic and Evolutionary Computation Conference Companion. GECCO '24 Companion (2076–2082). doi:10.1145/3638530.3664130.

60. Vaswani, A., Shazeer, N., Parmar, N., and et al. (2017). Attention is all you need. In: Proceedings of the 31st International Conference on Neural Information Processing Systems. NIPS'17 (6000–6010). URL: <https://dl.acm.org/doi/10.5555/3295222.3295349> accessed: 2025-9-22.

61. Munkhdalai, T., and Yu, H. (2017). Neural tree indexers for text understanding. In: Proceedings of the 15th Conference of the European Chapter of the Association for Computational Linguistics: Volume 1, Long Papers. (11–21). URL: <https://aclanthology.org/E17-1002> accessed: 2025-9-22.

62. Cybenko, G. (1989). Approximation by superpositions of a sigmoidal function. *Mathematics of Control, Signals and Systems* *2*, 303–314. doi:10.1007/BF02551274.

63. Hornik, K. (1991). Approximation capabilities of multilayer feedforward networks. *Neural Networks* *4*, 251–257. doi:10.1016/0893-6080(91)90009-T.

64. Fortin, F.-A., De Rainville, F.-M., Gardner, M.-A. G., Parizeau, M., and Gagné, C. (2012). Deap: Evolutionary algorithms made easy. *Journal of Machine Learning Research* *13*, 2171–2175. URL: <https://dl.acm.org/doi/10.5555/2503308.2503311>. Accessed: 2025-9-22.

Supplemental Information

A Reproducibility

Artifacts and environment. We release a self-contained artifact including exact scripts, configuration files, and experimental results. Experiments run on Python 3.9+ with DEAP⁶⁴-based typed GP, and baseline engines (PySR²⁷, Operon²⁵, PSTree²⁶, RILS-ROLS²⁸) as configured in the repository.

Determinism and seeds. Unless stated otherwise, each method/dataset is evaluated over 10 random seeds. We fix train/test splits per seed and log the seed alongside exports (per-seed metrics, expressions, and gate counts). This enables recomputation of the reported mean \pm std tables and figures.

Budget parity and complexity. To decouple search heuristics from primitive expressivity, engines are run under matched budgets (population/generations/time) and scored with a unified complexity metric (typed node count; constants included). CV proxies and warm-up schedules follow the same defaults across methods, as documented in the config files.

Self-checks and exports. The pipeline emits (i) raw and simplified expressions; (ii) per-seed test metrics (RMSE, MAE, R^2); (iii) Pareto pools with CV loss and complexity; (iv) gate-usage summaries; and (v) unit-aware thresholds (medians, IQR). Consistency checks enforce $\text{RMSE} \geq \text{MAE}$, and verify equality between internal vs. external metric computations to numerical tolerance.

Table S1: Software environments by method.

Environment	Specification
OS	Linux (kernel 6.8.0-84-generic), glibc (Ubuntu GLIBC 2.39-0ubuntu8.6)
Core (LGO / PySR / Operon) and utilities	Python 3.10.18; Python packages: numpy 2.2.5, pandas 2.3.2, scipy 1.16.1, scikit-learn 1.7.2, sympy 1.14.0, matplotlib 3.10.6. DEAP: deap 1.4.3; PySR: Julia 1.10, pysr 1.5.9. Operon: pyoperon 0.5.0, compiler: gcc \geq 9 or clang \geq 12. Implementation file: LGO_v2_1.py, PySR_v1.py, Operon_v1.py.
PSTree	Python 3.9.23; packages as in environment_pstree.yml. Implementation file: PSTree_v2_2.py.
RILS-ROLS	Python 3.11.13; packages as in environment_rils.yml. Implementation file: RILS_ROLS_v2_1.py.

Table S2: Artifact index.

Item	Reference
GitHub repo (public)	https://github.com/oudeng/LGO
Zenodo snapshot (DOI)	[ZENODO_DOI_URL]
Primary datasets	MIMIC-IV ICU (de-identified) ^{14–16} ; NHANES (CDC public release) ¹⁷
UCI datasets	CTG (Cardiotocography) ⁴⁹ ; Cleveland (Heart Disease numeric) ⁵⁰ ; Hydraulic (Condition Monitoring) ⁵¹
Entry script	run_v3_8.py
Seeds	1, 2, 3, 5, 8, 13, 21, 34, 55, 89
Baselines	PySR, Operon, PSTree, RILS-ROLS
Figure scripts	utility_plots/01_median_performance_violin.py, 02_pareto_front.py, 03_gating_usage.py, 04_thresholds.py
Configs	config/guidelines.yaml (anchors)
Canonical outputs	overall_(#dataset)/overall_metrics.csv, thresholds_units.csv, threshold_audit*.csv, top-1 expression dumps

Table S3: Operator sets and search budgets.

Method	Operator set	Budget / key options
LGO _{base}	Fundamental operators of {add, sub, mul, div, sqrt, log, pow}	pop=800, gen=100, tourn=7; $p_{cx} = 0.8$, $p_{mut} = 0.2$; CV proxy: disabled (weight=0.0; folds=2; sub-sample=0.30; warmup=0.80).
LGO _{soft}	LGO _{base} + soft-gating nodes (lgo, lgo_and2/or2, lgo_and3; gate_expr enabled)	typed mode=light; micro-mutation prob=0.10; local opt steps=60; other budgets aligned with LGO _{base} (pop/gen/tourn/cx/mut);
LGO _{hard}	LGO _{base} + hard-threshold node (lgo_thre) (+ AND/OR/gate_expr enabled)	as above (pop=800, gen=100, tourn=7; $p_{cx} = 0.8$, $p_{mut} = 0.2$).
PySR	unary/binary ops: unary_ops={sqrt}, binary_ops={+,-,*,/}	niterations=20 (derived from ngen=80), population_size=150 (derived from pop=600, using rule: max(128, pop/4)); loss: $(x - y)^2$ (MSE); maxsize=20, maxdepth=10, procs=1; complexity weights: +/ - /* : 1, / : 1.5, $\sqrt{\cdot}$: 1.5.
Operon	allowed symbols {add, sub, mul, div, sqrt, variable, constant}	population=600, generations=80; max_depth=10, max_size/max_length=30, n_threads=1; tournament / complexity penalty: library default (not explicitly set in wrapper; post-processing filters by CV loss and node count).
PSTree	piecewise symbolic tree + GP refinement	max_depth=10, max_leaf_nodes=32, min_samples_leaf=20; pop=600, gen=80.
RILS-ROLS	robust SR via iterated local search	max_fit_calls=100000, max_time=3600s, max_complexity=50, sample_size=1.0, complexity_penalty=1e-3.

Notes: This table reflects the aligned budgets. Budgets are identical across LGO variants (base/soft/hard); PySR/Operon use 600/80 under our wrapper (no pop/gen override in the command lines); PSTree is explicitly set to 600/80 with larger tree capacity. Complexity is reported via a unified node-count metric (functional nodes + terminals), while engine-native complexity is retained for within-method Pareto plots.

B Logistic-Gated Operators (LGO): formal definitions and properties

We denote the logistic function by

$$\sigma(z) = \frac{1}{1 + e^{-z}}.$$

Throughout, $x, y, z \in \mathbb{R}$ are feature-domain variables (Feat); $a \in \mathbb{R}_+$ is a positive steepness parameter (Pos); $b \in \mathbb{R}$ is a threshold in standardized (z-score) space (Thr). In implementation we use $a = \text{softplus}(\tilde{a})$ to enforce $a > 0$ and clip pre-sigmoid arguments to $[-60, 60]$ for numerical stability; b is clipped to $[-3, 3]$ in z-space.

Canonical 1-input gates (main-text Eq. (1)–(2)).

$$\text{LGO}_{\text{soft}}(x; a, b) = x \sigma(a(x - b)), \quad \text{LGO}_{\text{hard}}(x; a, b) = \sigma(a(x - b)).$$

We also use the shorthand $\text{gate}(u; a, b) = \sigma(a(u - b))$ and the expression-level gate

$$\text{gate_expr}(f; a, b) = f \text{ gate}(f; a, b).$$

Pairwise and multi-input variants (as in the code).

$$\begin{aligned} \text{LGO}_{\text{pair}}(x, y; a, b) &= (x y) \sigma(a((x - y) - b)), \\ \text{AND2}(x, y; a, b) &= (x y) \sigma(a(x - b)) \sigma(a(y - b)), \\ \text{OR2}(x, y; a, b) &= (x + y) \left(1 - (1 - \sigma(a(x - b))) (1 - \sigma(a(y - b)))\right), \\ \text{AND3}(x, y, z; a, b) &= (x y z) \sigma(a(x - b)) \sigma(a(y - b)) \sigma(a(z - b)). \end{aligned}$$

Limits and interpretation. Fix b . As $a \rightarrow \infty$,

$$\text{LGO}_{\text{hard}}(x; a, b) \rightarrow \mathbf{1}\{x > b\}, \quad \text{LGO}_{\text{soft}}(x; a, b) \rightarrow x \mathbf{1}\{x > b\},$$

pointwise and uniformly on compact sets avoiding $x = b$. Thus AND2 approaches the indicator of the axis-aligned rectangle $\{x > b, y > b\}$ (modulated by $x y$), while OR2 approaches $\mathbf{1}\{x > b \text{ or } y > b\}$ (modulated by $x + y$). See main-text Equation 1–2 for the canonical gates.¹

Gradients (used in local refinements). Let u be either a feature x or a subexpression $f(\cdot)$ and $s = \sigma(a(u - b))$. Then

$$\begin{aligned} \frac{\partial \text{LGO}_{\text{hard}}}{\partial a} &= (u - b) s(1 - s), & \frac{\partial \text{LGO}_{\text{hard}}}{\partial b} &= -a s(1 - s), \\ \frac{\partial \text{LGO}_{\text{soft}}}{\partial a} &= u(u - b) s(1 - s), & \frac{\partial \text{LGO}_{\text{soft}}}{\partial b} &= -a u s(1 - s). \end{aligned}$$

Expression-level gates use the chain rule with $u = f(\cdot)$.

Unit-aware inversion of thresholds. Evolution is carried out in standardized space. For a feature x with training-only statistics (μ_x, σ_x) and a learned z-threshold \hat{b} , the natural-unit threshold is

$$\hat{b}_{\text{raw}} = \mu_x + \sigma_x \hat{b}.$$

For $\text{gate_expr}(f; a, b)$ we estimate the z-standardization of f on the training fold and apply the same inversion. This mapping is used in all threshold audit tables and plots.

¹In code, `lgo_thre` implements LGO_{hard} ; `lgo` implements LGO_{soft} .

C Top-1 and Top-k expressions

C.1 From raw engine strings to the Simplified Expression

All engines output raw, typed strings with ephemeral constants (e.g., `add`, `mul`, `lgo_hard`, `gate_expr`). To render the human-readable equations reported in the main text, we apply a deterministic and auditable pipeline:

- (i) **Parsing and typing.** Raw strings are parsed into typed ASTs with three disjoint domains: `Feat` (feature values), `Pos` (positive steepness), and `Thr` (thresholds).
- (ii) **Constant folding and sanitization.** Algebraic constants are folded; numerically tiny subtrees are collapsed; denormals are clipped. Printing precision is unit-aware for display (e.g., `mmHg`: 1 decimal; `mmol/L`: 1 decimal; `mg/dL`: integer), while evaluation retains full precision.
- (iii) **Canonical rewrites (sound under typing).** We apply a small rewrite set (Table S4): neutral/absorbing removals ($\text{add}(x, 0) \rightarrow x$, etc.), associativity flattening, commutative sorting, and domain-safe identities ($\log(\exp x) \rightarrow x$, etc.).
- (iv) **Gate compaction and unit-aware thresholds.** $\text{lgo_hard}(x; a, b) \mapsto \text{gate}(x)$, $\text{lgo_soft}(x; a, b) \mapsto \text{gate}(x) \cdot x$, $\text{gate_expr}(f; a, b) \mapsto \text{gate}(f) \cdot f$. The learned threshold b_z is mapped to natural units by $\hat{b}_{\text{raw}} = \mu_x + \sigma_x b_z$ using training-only statistics (μ_x, σ_x) .
- (v) **Readability passes.** Factor repeated gates, linearize sums/products, and merge near-duplicate gates of the same feature when thresholds differ by less than a small tolerance (we keep the median).
- (vi) **Numeric equivalence check.** We require identical external metrics on the test split and a strict pointwise tolerance $\max_i |\hat{y}_i^{\text{raw}} - \hat{y}_i^{\text{simp}}| < 10^{-9}$. Expressions that fail this check are left less simplified and flagged in the SI artifact.

Table S4: Canonical rewrite rules used in expression simplification.

Rule	Condition / Note
$\text{add}(x, 0) \rightarrow x$, $\text{mul}(x, 1) \rightarrow x$, $\text{mul}(x, 0) \rightarrow 0$	Neutral/absorbing removal
$\text{div}(x, 1) \rightarrow x$, $\text{pow}(x, 1) \rightarrow x$, $\text{pow}(x, 0) \rightarrow 1$	Domain valid
$\text{sqrt}(\text{pow}(x, 2)) \rightarrow x$	Sound when $x \geq 0$ (Pos/non-neg.)
$\log(\exp x) \rightarrow x$, $\exp(\log x) \rightarrow x$	Domain preserved ($x > 0$)
Flatten <code>add/mul</code> ; sort commutative args	Canonical, improves readability
$\text{lgo_soft}(x; a, b) \rightarrow \text{gate}(x) \cdot x$	Gate compaction
$\text{lgo_hard}(x; a, b) \rightarrow \text{gate}(x)$	Probabilistic gate
$\text{gate_expr}(f; a, b) \rightarrow \text{gate}(f) \cdot f$	Expression-level gating

C.2 Worked examples: ICU and NHANES (Top-1)

ICU (composite risk). The LGO_{hard} top-1 model on this split prunes gates and simplifies to a smooth form:

Raw (snippet)

```
add(c0, mul(c1, sqrt(lactate_mmol_l)), mul(c2, vasopressor_use_std), ...)
```

Simplified (reported in the main text):

$$\hat{y} \approx \alpha_0 + \alpha_1 \sqrt{\text{Lactate}} + \alpha_2 \text{Vasopressor.}$$

This is consistent with our parsimony analysis: when gates do not improve external metrics under the budget, LGO_{hard} reduces to smooth primitives.

NHANES (metabolic score). By contrast, the LGO_{hard} top-1 contains multiple explicit gates that match our threshold-audit:

Raw (snippet)

```
add(gate_expr(mul(triglycerides,c1),a_tg,b_tg_z),  
lgo_hard(fasting_glucose,a_fg,b_fg_z),  
lgo_hard(systolic_bp,a_sbp,b_sbp_z),  
lgo_hard(inv(hdl_cholesterol),a_hdl,b_hdl_z),  
lgo_hard(waist_circumference,a_wc,b_wc_z), ...)
```

Simplified (reported in the main text):

$$\hat{y} \approx \text{gate}(\text{TG}) + \text{gate}(\text{FG}) + g(\text{SBP}, \text{HDL}, \text{Waist}),$$

with thresholds mapped to natural units and compared to guideline anchors.

C.3 Lightweight top- k audit

To complement top-1 exemplars, we summarize the top- k candidate pool per dataset (default $k = 100$) using the existing aggregated results shipped with the artifact:

- **Gate selectivity and sparsity.** From aggregated / gating_usage_*.csv, we report (i) the fraction of models that contain at least one gate (% with gates) and (ii) the median number of gates per model (zeros included). Table S5 consolidates these statistics. These results mirror the main-text trend: LGO_{hard} keeps high usage where warranted (ICU, NHANES) and prunes gates otherwise (subset of Cleveland), while realizing fewer gates per model than LGO_{soft} .
- **Feature-wise gate incidence and threshold agreement.** Using aggregated / thresholds_units_*.csv and aggregated / threshold_audit_summary_*.csv, we list the most frequently gated features (Top-3 to Top-5), together with the median threshold (natural units), IQR, and the share of models whose gates fall within $\leq 10\% / \leq 20\%$ of anchors. Table S6 summarizes ICU; Table S7 summarizes NHANES. No additional plotting is required.

Across Top- k candidates, LGO_{hard} exhibits selective gate usage and sparser switching structure than LGO_{soft} , while the recovered thresholds — mapped to natural units — cluster near clinical anchors on ICU and NHANES. These pool-level trends corroborate the top-1 exemplars and the main-text threshold-audit.

Table S5: Top- k gate usage and sparsity (aggregated; $k = 100$).

Dataset	Experiment	Top- k	Gate usage (%)	Median # gates	Complexity (median)	CV loss (median)
ICU	base	100	0.0	0.0	36.00	0.6447
ICU	lgo_hard	100	90.0	4.0	52.50	0.6223
ICU	lgo_soft	100	100.0	10.0	67.75	0.9767
NHANES	base	100	0.0	0.0	36.00	0.5941
NHANES	lgo_hard	100	100.0	5.0	53.00	0.4583
NHANES	lgo_soft	100	100.0	12.5	72.15	0.7449

Table S6: ICU (Top- k) most frequently gated features with unit-aware thresholds (natural units).

Dataset	Feature	Unit	Gate	Models w/ gate		Threshold			Gate
				cnt	N	%	Median	Q1	
ICU	lactate_mmol_l	mmol/L	10	10	10	1.91	1.91	1.91	lgo_thre
ICU	vasopressor_use_std	(std)	7	7	7	0.10	0.10	0.10	lgo_thre
ICU	map_mmhg	mmHg	6	6	6	63.71	63.71	63.71	lgo_thre
ICU	mechanical_ventilation_std	(std)	5	5	5	0.04	0.04	0.04	lgo_thre
ICU	respate_max	min ⁻¹	3	3	3	27.04	27.04	27.04	lgo_thre

Table S7: NHANES (Top- k) most frequently gated features with unit-aware thresholds (natural units).

Dataset	Feature	Unit	Gate	Models w/ gate		Threshold			Gate
				cnt	N	%	Median	Q1	
NHANES	waist_circumference	cm	31	31	31	93.94	91.67	98.02	lgo_thre
NHANES	systolic_bp	mmHg	28	40	40	128.34	128.34	128.89	lgo_thre
NHANES	fasting_glucose	mg/dL	24	37	37	85.45	74.54	95.40	lgo_thre
NHANES	gender_std	(std)	21	20	20	0.27	0.27	0.27	lgo_thre
NHANES	hdl_cholesterol	mg/dL	3	3	3	39.65	39.65	39.65	lgo_thre

D Anchors and unit metadata

Purpose. To support unit-aware audit, we curate dataset-specific anchors (clinical cut-points) and units in YAML files: `config/guidelines.yaml`. Anchors let us compare learned thresholds against domain references (e.g., SBP 120–130 mmHg, lactate 2 mmol/L, fasting glucose 100/126 mg/dL)^{8,9,12}.

Schema. Each entry binds a feature name (matching the processed dataset) to a unit string and an anchor value:

```
feature_name:  
  unit: "mmHg"  
  anchor: 130.0  
  note: "ACC/AHA threshold for elevated SBP"
```

Units follow the display conventions used in the main text (e.g., mmHg, mg/dL, mmol/L, cm). If a feature is a standardized state indicator, we mark unit as "(std)".

Curation and provenance. ICU anchors derive from the Surviving Sepsis Campaign and ICU monitoring practice⁸; NHANES anchors reflect ACC/AHA blood pressure guidance⁹ and ADA diagnostic thresholds for glucose¹². YAML also includes some brief `note` fields for citation/context.

Integration in audit. During analysis, thresholds learned in z -space are mapped to natural units using training-only statistics. We then compute the relative deviation $|\hat{b}_{\text{raw}} - b_{\text{anchor}}|/|b_{\text{anchor}}|$ and color cells (green $\leq 10\%$, yellow $\leq 20\%$, red $> 20\%$). Features lacking anchors are omitted from agreement plots to avoid gray (N/A) clutter.

Coverage and maintenance. YAML includes only features present in a given dataset to avoid mismatches; we validate names programmatically before audit. Anchors are versioned within the repository; updates require a brief provenance note and citation. The pipeline emits a coverage report listing anchored vs. unanchored features to aid curation.

Limitations. Anchors capture reference cut-points, which may differ from operational alerting thresholds (e.g., ICU respiratory rate alarms). We therefore report both the learned threshold distribution (median/IQR) and the anchor, and discuss plausible context-driven deviations in the main text.

E Pareto and complexity

Definitions. Complexity counts typed primitive nodes (operators, variables, constants). CV loss denotes the cross-validation proxy used during search (folds, warm-up, and subsampling as in the shared config). Pareto fronts are formed by non-dominated solutions in (CV loss, complexity) space from the top- k pool (here $k = 100$).

Protocol. For each method/dataset we collect the top- k candidates by the engine’s internal score, recompute CV loss with the shared proxy, and remove dominated points. We then plot the surviving front with color indicating method and marker size indicating (optionally) test performance for reference.

Reading guide. Lower-left regions (low CV loss, low complexity) indicate preferable accuracy–simplicity trade-offs. On ICU and NHANES, LGO_{hard} populates fronts at reduced complexity relative to soft gates, consistent with the gate-usage statistics. On predominantly smooth tasks, LGO variants prune gates and align with smooth baselines.

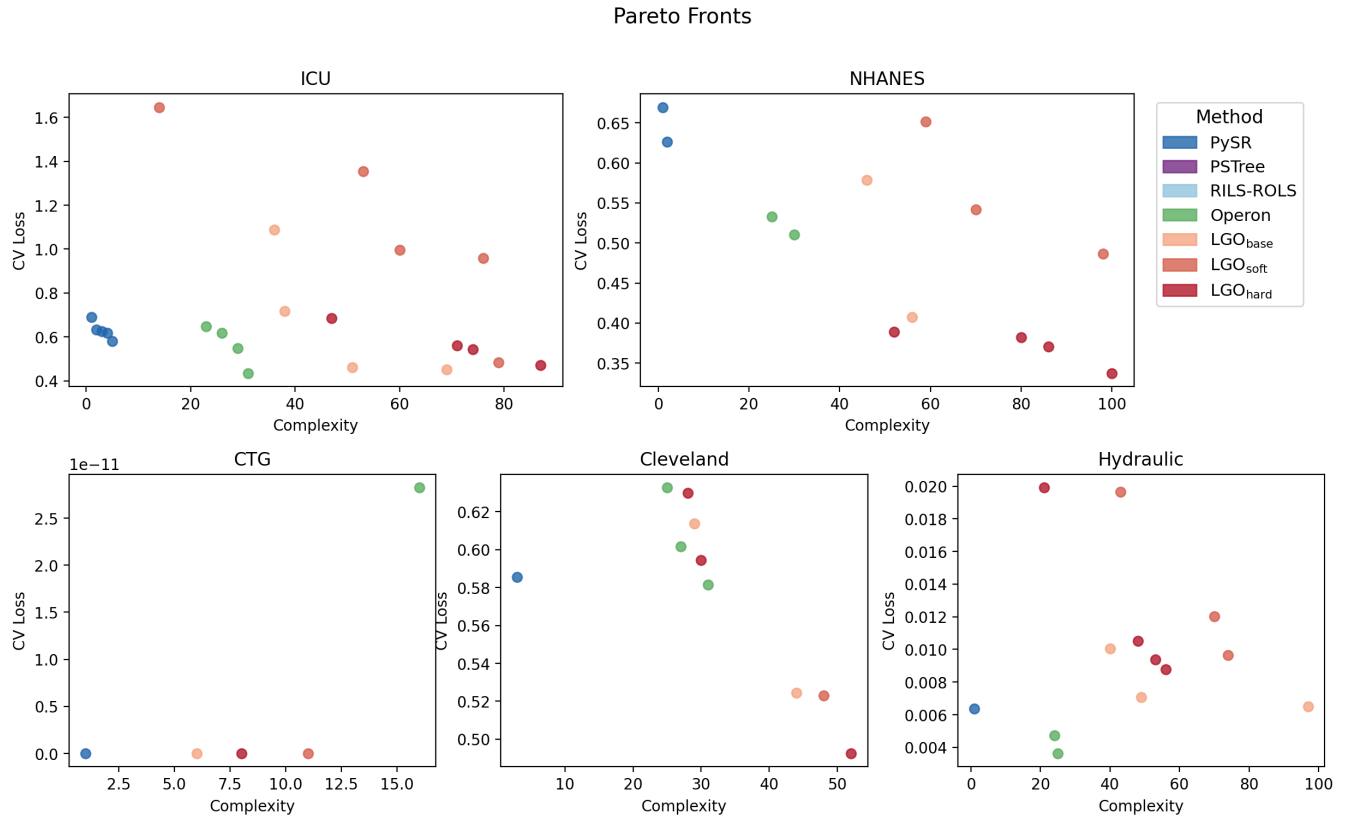


Figure S1: Extended Pareto fronts (CV loss vs. symbolic complexity). One panel per dataset. Points are non-dominated candidates aggregated across seeds. ICU/NHANES: LGO_{hard} yields competitive low-loss candidates at moderate complexities; LGO_{soft} is broader and typically less favorable. CTG: near-separable, fronts are saturated. Cleveland: LGO_{hard} reaches the lowest loss at higher complexity, Operon trades slightly higher loss for lower complexity. Hydraulic: smooth relations favor RILS-ROLS/Operon. Complexity is computed with a unified node count; CV-loss uses the same proxy across methods (details in Table S3).

F UCI benchmarks

Task characterization. CTG (binary) is near-separable with histogram features; Cleveland (regression) presents moderate signal with mixed clinical covariates; Hydraulic (regression) is dominated by smooth sensor-response relationships.

Summary. CTG yields ceiling AUROC/AUPRC for multiple engines; LGO variants match the ceiling with compact formulas. On Cleveland, LGO_{hard} is competitive with Operon and exposes auditable thresholds on age/cholesterol/thalach ranges. On Hydraulic, RILS-ROLS excels as expected for smooth relations; LGO_{hard} underperforms when thresholded regimes are weak. Full mean \pm std tables are provided below; per-seed metrics and expressions are in the artifact.

Table S8: UCI CTG NSPbin: mean \pm std (10 seeds).

method	experiment	AUROC \uparrow	AUPRC \uparrow	Brier \downarrow
PySR	base	1.000 \pm 0.000	1.000 \pm 0.000	0.211 \pm 0.000
PSTree	base	0.766 \pm 0.014	0.526 \pm 0.035	0.386 \pm 0.018
RILS-ROLS	base	0.517 \pm 0.135	0.288 \pm 0.110	0.333 \pm 0.164
Operon	base	1.000 \pm 0.000	1.000 \pm 0.000	0.211 \pm 0.000
LGO	base	1.000 \pm 0.000	1.000 \pm 0.000	0.211 \pm 0.000
LGO	LGO_{soft}	1.000 \pm 0.000	1.000 \pm 0.000	0.212 \pm 0.002
LGO	LGO_{hard}	1.000 \pm 0.000	1.000 \pm 0.000	0.211 \pm 0.000

Table S9: UCI Heart Cleveland num: mean \pm std (10 seeds).

method	experiment	$R^2 \uparrow$	RMSE \downarrow	MAE \downarrow
PySR	base	0.416 \pm 0.105	0.909 \pm 0.085	0.638 \pm 0.070
PSTree	base	0.075 \pm 0.275	1.132 \pm 0.122	0.711 \pm 0.096
RILS-ROLS	base	0.392 \pm 0.127	0.928 \pm 0.109	0.645 \pm 0.071
Operon	base	0.480 \pm 0.107	0.856 \pm 0.075	0.600 \pm 0.059
LGO	base	0.436 \pm 0.112	0.892 \pm 0.084	0.574 \pm 0.067
LGO	LGO_{soft}	0.397 \pm 0.177	0.914 \pm 0.108	0.583 \pm 0.076
LGO	LGO_{hard}	0.484 \pm 0.118	0.852 \pm 0.090	0.531 \pm 0.061

Table S10: UCI HydraulicSys fault score: mean \pm std (10 seeds).

method	experiment	$R^2 \uparrow$	RMSE \downarrow	MAE \downarrow
PySR	base	0.738 \pm 0.031	0.089 \pm 0.004	0.069 \pm 0.004
PSTree	base	0.538 \pm 0.064	0.116 \pm 0.014	0.090 \pm 0.013
RILS-ROLS	base	0.946 \pm 0.007	0.040 \pm 0.004	0.028 \pm 0.002
Operon*	base	0.822 \pm 0.049	0.072 \pm 0.010	0.055 \pm 0.008
LGO	base	0.609 \pm 0.119	0.106 \pm 0.017	0.084 \pm 0.015
LGO	LGO_{soft}	0.397 \pm 0.215	0.131 \pm 0.024	0.106 \pm 0.021
LGO	LGO_{hard}	0.364 \pm 0.248	0.134 \pm 0.027	0.107 \pm 0.023

Notes: Two seeds excluded due to implausible R^2 values (< -1).